RESEARCH PAPER

PCCP
www.rsc.org/pccp

Sr diffusion in undoped and La-doped $SrTiO_3$ single crystals under oxidizing conditions†

Karsten Gömann,*[a] Günter Borchardt,[a] Michał Schulz,[a] Anissa Gömann,[b] Wolfgang Maus-Friedrichs,[b] Bernard Lesage,[c] Odile Kaïtasov,[d] Susanne Hoffmann-Eifert[e] and Theodor Schneller[f]

[a] *Institut für Metallurgie, Technische Universität Clausthal, Robert-Koch-Str. 42, D-38678 Clausthal-Zellerfeld, Germany. E-mail: karsten.goemann@tu-clausthal.de; Fax: +49 5323 72-3184; Tel: +49 5323 72-3688*
[b] *Institut für Physik und Physikalische Technologien, Technische Universität Clausthal, Leibnizstr. 4, D-38678 Clausthal-Zellerfeld, Germany*
[c] *Laboratoire d'Etude des Matériaux Hors Equilibre, Université Paris-Sud, F-91405 Orsay Cedex, France*
[d] *Centre de Spectrométrie Nucléaire et de Spectrométrie de Masse, Université Paris-Sud, F-91405 Orsay Cedex, France*
[e] *Institut für Festkörperforschung, Forschungszentrum Jülich, D-52425 Jülich, Germany*
[f] *Institut für Werkstoffe der Elektrotechnik II, RWTH Aachen, Sommerfeldstr. 24, D-52074 Aachen, Germany*

Received 15th December 2004, Accepted 3rd March 2005
First published as an Advance Article on the web 21st March 2005

Strontium titanate $SrTiO_3$(100), (110), and (111) single crystals, undoped or donor doped with up to 1 at% La, were isothermally equilibrated at temperatures between 1523 and 1773 K in synthetic air followed by two different methods of Sr tracer deposition: ion implantation of ^{87}Sr and chemical solution deposition of a thin $^{86}SrTiO_3$ layer. Subsequently, the samples were diffusion annealed under the same conditions as before. The initial and final depth profiles were measured by SIMS. For strong La-doping both tracer deposition methods yield similar Sr diffusion coefficients, whereas for weak doping the tracer seems to be immobile in the case of ion implantation. The Sr diffusivity does not depend on the crystal orientation, but shows strong dependency on the dopant concentration supporting the defect chemical model that under oxidizing conditions the donor is compensated by Sr vacancies. A comparison with literature data on Sr vacancy, Ti, and La diffusion in this system confirms the concept that all cations move *via* Sr vacancies. Cation diffusion is several orders of magnitude slower than oxygen diffusion.

1. Introduction

Strontium titanate $SrTiO_3$ is not only a model material for perovskite-type ternary oxides (ABO_3) but also has various technical applications, for example as electronic material (see, *e.g.*, ref. 1). It exhibits no phase transitions up to the melting point of *ca.* 2000 °C. By doping the electrical characteristics may be tailored to meet specific needs. By adding donors like the rare earth elements on the A site or Nb or Ta on the B site a promising material for resistive oxygen sensors is obtained which may be operated at temperatures above 1000 °C in a wide range of oxygen partial pressure, $p(O_2)$. The advantage of donor doped compared to acceptor doped $SrTiO_3$ is the unambiguous relation between electrical conductivity and $p(O_2)$ at higher $p(O)_2$ values. However, in contrast to acceptor doped $SrTiO_3$ where the highly mobile electrons, holes, and oxygen vacancies are the majority charge carriers and the system is well understood (see *e.g.*, ref. 2), in the case of donor doped material also cation vacancies are involved in the equilibration reactions after a change in $p(O_2)$ at high temperature. This leads to surface reconstruction and secondary phase formation, which besides the temperature and the $p(O_2)$ also depends on the crystal orientation and the dopant concentration (see *e.g.*, refs. 3 and 4, and references therein).

Following the defect chemistry model of donor doped $SrTiO_3$,[5] the bulk defect chemistry is determined by the reaction (see ref. 6 for defect notation)

$$O_O^{\times} \Leftrightarrow V_O^{\bullet\bullet} + 2e' + \frac{1}{2}O_{2(g)}. \quad (1)$$

Hence, an increase of the outer $p(O)_2$ causes a corresponding decrease in the oxygen vacancy and electron concentration. To compensate for the donor doping, cation vacancies are generated in return. Electrical conductivity and gravimetrical measurements,[7,8] determinations of the O uptake during the compensation change,[9] the Sr vacancy formation observed in solid solutions of $SrTiO_3$ and $La_{2/3}TiO_3$[10] and experiments on the secondary phase formation on different (Sr, La)TiO_3 stoichiometries[11] all provide experimental evidence that exclusively Sr vacancies are generated at least at dopant fractions below 0.3. Furthermore, computer simulation studies show that formation of the highly charged Ti vacancies is energetically very costly.[12] Because of the high packing density of the crystal lattice, interstitial sites virtually do not exist. As only one computer simulation study favours the compensation by a complete Schottky reaction,[13] Sr vacancy compensation is assumed throughout this paper.

† Presented at the 84th International Bunsen Discussion Meeting on the Structure and Dynamics of Disordered Ionic Materials, Münster, Germany, October 6–8, 2004.

DOI: 10.1039/b418824a

Upon the generation of Sr vacancies an excess of Sr ions is created. Some authors postulated the formation of Ruddlesden–Popper phases ($SrO \cdot nSrTiO_3$,[14]) as layers in the crystal as a sink for the excess Sr.[15,16] However, these phases have not been detected experimentally up to now. Newer results indicate that the formation of Sr vacancies is restricted to the crystal surface[17] and all excess Sr migrates to the surface where secondary SrO_x phases grow on top of the surface (see, *e.g.*, refs. 3, 18 and 19) following the reaction

$$Sr_{Sr}^{\times} + 2e' + \frac{1}{2}O_{2(g)} \Leftrightarrow V_{Sr}'' + SrO_{sec-phase} \qquad (2)$$

Additionally, Ruddlesden–Popper phases are formed at the surface in-between the secondary phases.[20,21]

In the crystal bulk, the Sr vacancy concentration is under oxidizing conditions fixed by the donor content

$$[D^{\bullet}] = 2[V_{Sr}''] \qquad (3)$$

leading to the observed correlation of the amount of secondary phases and the dopant concentration. The rate-limiting step of the equilibration after a change in $p(O_2)$ is therefore the diffusion of Sr vacancies from the surface into the crystal volume. As the Sr vacancy diffusivity is orders of magnitude lower than the diffusivites of both the oxygen vacancies and the electrons, a space charge zone develops in the near-surface region affecting the defect mobilities.[17]

In the opposite case of reduction at low $p(O_2)$, the oxygen release into the gas phase is accompanied by an electron generation. This leads to a partial reduction of Ti^{4+}. Also, the formation of Ti^{3+} containing phases like Ti_2O_3 or $LaTiO_3$ is observed.[22–24]

Although the defect chemical model seems to be consistent, reliable experimental data for the crucial parameter of the system, the Sr diffusivity, is not yet available. Decades ago, an experimental study on Sr and Ti diffusion in undoped $SrTiO_3$ focussing on the dislocation dependence[25] was published, which was confined to a single temperature of 1875 °C and did also not address the dopant concentration dependency. For the Sr vacancy diffusion, only one experimental study was published for Nb-doped (Sr, Ca)TiO_3,[26] but the effect of the different chemical composition regarding the Ca on the defect mobilities is not known. Another value for the Sr vacancy diffusivity was deduced indirectly from the depth-dependent O diffusion coefficient.[17,27] In this work, following investigations of the La, Nd, and Ti diffusion in La-doped $SrTiO_3$ under oxidizing conditions,[28,29] we present the results of Sr tracer diffusion experiments.

2. Experimental

Commercial $SrTiO_3$ single crystals were obtained from Crystec (Berlin, Germany). The different dopant concentrations and crystal orientations of the samples and the temperature ranges of the experiments will be given together with the two different tracer deposition procedures below. All anneals were carried out in an alumina tube furnace in a continuous flow of 10 cm^3 min^{-1} synthetic air (dry, 20% O_2, 80% N_2) at ambient pressure. Prior to tracer deposition the samples were annealed under the same conditions as the diffusion anneals to equilibrate the samples to a sufficient depth with the atmosphere of the respective experiment.

The samples were transferred to and from the furnace using a linear translator in steps of 10 cm min^{-1} and cooled in air. The time the samples resided in the hot zone of the furnace was taken to be the annealing duration. As the samples do not reach the annealing temperature immediately and diffusion also occurs to some extent during the cooling of the sample, this is an approximation. The samples reach room temperature not until 30 min after the experiment. By using a sample holder equipped with a thermocouple, we recorded the sample holder temperature during the transfer. By integrating over the heating and cooling periods using the temperature dependent D values given in section 3.3, a Sr diffusion length of *ca.* 1 nm at 1573 K and 2 nm at 1673 K is obtained for strongly doped samples. For weakly doped samples, these values are even about a decade lower. Therefore, no diffusion length correction was applied.

As described in section 1, annealing under oxidizing conditions leads to an epitaxial growth of secondary SrO phases on top of the surface, in particular on strongly doped samples. Optical micrographs of surfaces similar to the samples used in this work are shown in ref. 29. To remove these SrO islands after equilibration, the 1 at% doped samples were washed for 24 h at 60 °C in deionized water. Hereby, the majority of the islands is removed (see again ref. 29).

For tracer deposition *via* ion implantation, $SrTiO_3$ crystals with dimensions of 5 × 5 × 1 mm^3, the crystallographic orientations (100), (110), and (111), and with La concentrations of 0.02 or 1 at% were (pre-)annealed at temperatures between 1523 and 1723 K for up to 40 days. The tracers, $^{87}Sr^+$ ions, were implanted in the samples with a fluence of 2×10^{16} cm^{-2} at an accelerating voltage of 100 keV and at room temperature.

During implantation, the impinging ions cause significant damage to the $SrTiO_3$ crystal lattice causing, for instance, forward implantation or sputtering of lattice ions. Depending on the implantation dose, this creates a high amount of vacant lattice sites and can lead to an amorphization of the implanted depth region of the sample. Comparable amorphized $SrTiO_3$ layers can be recrystallized by annealing in oxidizing atmosphere for 30 min to several hours at temperatures of 1050–1100 °C.[30,31] Therefore, the samples were annealed after implantation for 30 to 60 min at temperatures of at least 1050 °C.

Additionally, $SrTiO_3$(100) crystals with dimensions of 10 × 10 × 1 mm^3, undoped or with La concentrations of 0.02 or 1 at%, were equilibrated for up to four weeks at temperatures between 1573 and 1773 K. Subsequently, polycrystalline undoped $SrTiO_3$ layers enriched to *ca.* 95% in ^{86}Sr were deposited as tracer source for Sr diffusion experiments on the samples by means of spin coating chemical solution deposition (CSD). 0.1 molar solutions were prepared from ^{86}Sr-carbonate and Ti-butoxide precursors *via* the acetate route.[32,33] A slight Ti excess of 0.5% was adjusted to prevent the formation of additional Sr bearing phases. Five subsequent coating steps were performed on each substrate. After each step the samples were annealed for 10 min at 700 °C in oxygen atmosphere. Finally, the samples were annealed for 30 min at 750 °C in oxygen atmosphere. Using optical microscopy and scanning electron microscopy (SEM) equipped with an energy dispersive X-ray spectrometer (EDX) the layers appeared to be dense and chemically uniform.

The depth distribution of all ions was measured before and after the diffusion anneals by secondary ion mass spectrometry (SIMS). The majority of the measurements was done with a Cameca IMS 3f using a 10 keV O^- primary ion beam and a primary current of 30 to 100 nA. Depending on the secondary ion intensities, an area with a diameter of *ca.* 10–60 μm in the center of the sputtered area of 250 × 250 μm^2 was gated for signal detection. For some of the measurements, a Cameca IMS 4f or IMS 5f were used, both with a Cs^+ primary beam operated at 10 keV and 15 nA with a scanned area of about 150 × 150 μm^2, detecting secondary positive ions at a potential of 3.8 keV.

In general, the isotopes ^{12}C, ^{16}O, ^{48}Ti, ^{86}Sr, ^{87}Sr, and ^{88}Sr were recorded, each with a counting time of 1 s. Additionally, ^{139}La was analyzed on all La-doped samples. In most cases, also the mass 89 was analyzed to check for the formation of ^{88}SrH and thus for possible hydride interferences between the different Sr isotopes (*e.g.*, the interference of ^{86}SrH on ^{87}Sr). Hydride formation is found to be strongest at the beginning of

the depth profile. In most cases the value for the intensity ratio $^{88}SrH/Sr$ was less than 10^{-3} and hydride interferences were therefore negligible. For some measurements done at the IMS 4f instrument where this ratio exceeded 10^{-2} the interferences were corrected mathematically afterwards. The energy slit was usually fully opened to prevent oscillating signals due to the slight charging of the insulating samples.

Prior to SIMS analysis, all samples were coated with a carbon layer of 10 to 50 nm thickness to prevent charging. As the samples were used for several consecutive experiments, carbon is preferable to metals like Au because it reacts to CO_2 and is removed at the beginning of the next diffusion anneal. This was verified performing X-ray photoelectron spectroscopy (XPS) using an Al Kα beam on a carbon coated $SrTiO_3$ sample before and after annealing for 2 h at 1573 K. Prior to annealing, a strong C 1s peak is visible at a binding energy of 284 eV indicating atomic carbon. No peaks of Sr, Ti, or La are detected, which is understandable considering the carbon layer thickness of at least 10 nm and the information depth of XPS of *ca.* 2.5 nm for Sr 3d in carbon. After annealing, Sr, Ti, and La peaks appear in the spectrum and the intensity of the C 1s peak, which is still at the same position at 284.5 eV, is strongly reduced. The formation of carbonates at the surface can be excluded, as in carbonates the C 1s peak is located at higher binding energies of about 290 eV. As the analysed area of the respective XPS instrument slightly exceeds our sample size, contributions of the sample holder are visible in the spectrum. It is made from Mo metal, which possesses a high solubility for C. Therefore, an additional XPS spectrum of only the Mo holder without the $SrTiO_3$ sample was recorded, which verified that the remaining C signal in the spectrum can be fully attributed to the sample holder.

The crater depths were measured using a surface profiler (Tencor AlphaStep500). For all profiles used in the following, the depth was corrected by subtraction of the conducting carbon layer. In cases where the carbon layer thickness was sufficiently low compared to the overall crater depth, a linear depth calibration was used. At carbon layer thicknesses above *ca.* 30 nm a second depth profile of only the carbon layer was recorded which was used to correct the depth according to the different sputter rates of the carbon layer and the $SrTiO_3$ crystals.

3. Results and discussion

3.1. Ion implantation

After implantation, the tracer ions ideally show a Gaussian distribution following the expression,[34]

$$c(x,t) = \frac{N}{\sqrt{2\pi\sigma^2}} \exp\left(-\frac{(x-x_c)^2}{2\sigma^2}\right) \qquad (4)$$

with c being the tracer concentration, x the depth, t the time, N the implanted dose, σ the standard deviation of the Gauss distribution and x_c the mean value of the projected range.

Annealing of the implanted samples leads to tracer diffusion which can be determined from the broadening of the Gaussian profile. The tracer diffusion coefficient D is derived directly from the increase in σ by fitting the proper solution of Fick's second law to the depth profiles:

$$c(x,t) = \frac{N}{\sqrt{2\pi(\sigma^2+2Dt)}} \exp\left(-\frac{(x-x_c)^2}{2\sigma^2+4Dt}\right) \qquad (5)$$

yields:

$$D = \frac{\sigma_{post}^2 - \sigma_{pre}^2}{2t}, \qquad (6)$$

where σ_{pre} and σ_{post} are the values for σ measured before and after an annealing step.

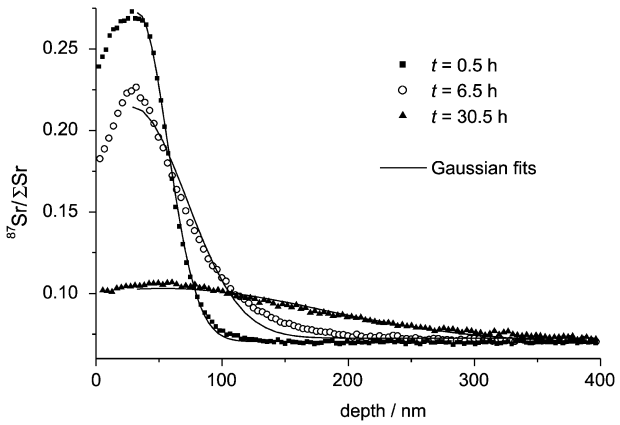

Fig. 1 ^{87}Sr depth profiles recorded with SIMS on a 1 at% La-doped $SrTiO_3$(100) single crystal implanted with $^{87}Sr^+$. t: annealing duration at $T = 1673$ K.

In Fig. 1, typical depth profiles of an ion implanted sample doped with 1 at% La are shown. After annealing the expected broadening of the tracer distribution is observed. Judging from the distorted shape of the tracer profiles at depths $x < x_c$, the recovery of the implantation damage by recrystallisation of the $SrTiO_3$ lattice seems to be incomplete in this region, causing a different diffusion behaviour of the Sr tracer at $x < x_c$. A similar behaviour was observed with implanted La tracers.[28] In contrast, identical experiments with Nd and Ti tracers[28,29] did not lead to distorted profiles. The depth distribution of the vacant lattice sites generated by the irradiation possesses a similar shape as the implanted ions, but the maximum is shifted to a lower depth. Therefore the radiation damage is strongest at $x < x_c$. Calculating the number of vacancies generated by each implanted ion using the SRIM 2003 software package ("the stopping and range of ions in matter", see ref. 35) yields values of about 680 vacancies/ion for ^{49}Ti, 1100 vacancies/ion for ^{87}Sr, and 1700 vacancies/ion for ^{139}La implantation for the respective acceleration voltages. Considering that the implanted dose was twice as high in the case of Sr compared to Ti and La the amount of radiation damage should be much higher in the case of Sr and La compared to Ti. Therefore, only the profile sections with $x \geq x_c$ were used for fitting.

Another slight deviation from the ideal Gauss shape is observed at the trailing edge of the implantation profiles at ^{87}Sr isotope fractions below 0.1. This is caused by atomic mixing due to the recoil of sample ions during the SIMS analyses (see *e.g.*, ref. 36). As the D values were determined from the difference in the σ values of the depth profiles as described above, these deviations have no significant influence on the determined D values[29,37] and were therefore neglected.

In Fig. 1, the Gauss fit to the profile after 30 min of annealing yields $x_c = 33.1$ nm and $\sigma = 23.6$ nm. Calculating the respective values with the SRIM 2003 software and assuming a stoichiometric $SrTiO_3$ crystal with a density of 5.12 g cm^{-3} gives a similar x_c value of 33.9 nm but a much lower σ value of 13.1 nm. This difference is caused by the surface roughness and atomic mixing during the SIMS analysis (see above) and additionally by tracer diffusion during the 30 min of annealing. As stated earlier, a high amount of vacancies is present at the beginning of the annealing experiment due to radiation damage. Under these conditions, the Sr tracer diffusivity might be much higher compared to the values obtained later after damage recovery.

Fig. 2 shows typical depth profiles of a weakly doped sample. Whereas some outward diffusion of the tracer ions seems to occur in the damaged profile section at depths $x < x_c$, no significant diffusion could be detected at $x \geq x_c$ even after several weeks of annealing. Therefore, only an upper limit of the Sr tracer coefficient, D, can be calculated from the

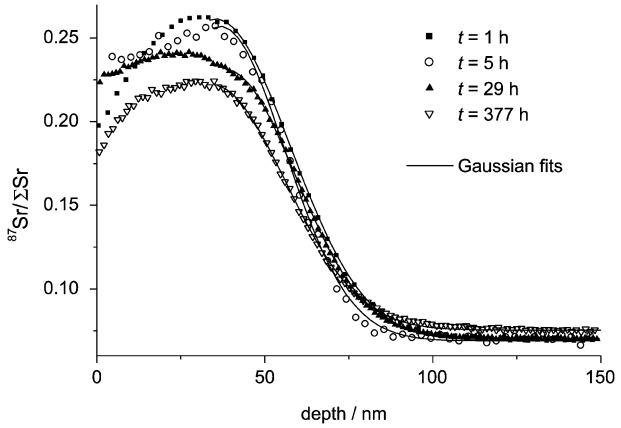

Fig. 2 ^{87}Sr depth profiles recorded with SIMS on a 0.02 at% La-doped $SrTiO_3$(100) single crystal implanted with $^{87}Sr^+$. t: annealing duration at $T = 1573$ K.

annealing duration and the analytical error. The latter, more precisely the standard deviation s of the analytical reproducibility of the depth profiles, which is mainly determined by errors in the mechanical crater depth measurement and the Gaussian fit, can be calculated from the single measurements of each weakly doped sample using the expression[38]

$$s^2 = \frac{\sum_{j=1}^{N}\sum_{i=1}^{n}(\sigma_{ij} - \overline{\sigma}_j)^2}{\sum_{j=1}^{N}(n_j - 1)} \qquad (7)$$

with σ_{ij} being a single value, σ_j the mean value, and n the number of values of sample j and N the number of samples. The σ values of the weakly doped samples compiled in Table 1 yield a value of $s = 1.45$ nm. Hence, using $2s$ as analytical error, the Sr tracer diffusion coefficients must be lower than 6.9×10^{-23} m^2 s^{-1} at $T = 1573$ K, and 7.6×10^{-23} m^2 s^{-1} at $T = 1673$ K, respectively.

The σ and D values obtained for the strongly doped samples are listed in Table 2. The D values will be discussed together with the results of the second tracer deposition method in section 3.3.

3.2. Chemical solution deposition

Fig. 3 displays depth profiles of a 1 at% La-doped sample directly after deposition of the polycrystalline $^{86}SrTiO_3$ layer ($t = 0$) and after two annealing steps.

At $t = 0$, a uniform ^{86}Sr enrichment of 95.7% is observed in the layer, which drops approximately to the natural abundance of 9.86% in the $SrTiO_3$ crystal. ^{88}Sr, which has the highest natural abundance of 82.58, shows an opposite distribution with values of 3.1% in the layer and 81.6% in the crystal. ^{87}Sr, which is not displayed in Fig. 3, shows a similar behaviour as

Table 1 σ values [see eqn. (4)] of the 0.02 at% La-doped $SrTiO_3$ samples implanted with $^{87}Sr^+$. $\sigma(t)$: value measured after the respective annealing time t; $\bar{\sigma}$: average σ value

	$\bar{\sigma}$/nm	$\sigma(t)$/nm				
t at $T = 1573$ K		1 h	+4 h	+1 d	+14.5 d	+32.5 d
$SrTiO_3$(100)	26.4	26.5	26.5	29.4	23.1	—
$SrTiO_3$(110)	31.4	—	31.4	31.2	—	31.7

t at $T = 1673$ K		0.5 h	+24 h	+27 d
$SrTiO_3$(100)	28.0	28.9	27.4	27.7
$SrTiO_3$(110)	26.6	28.8	26.0	25.0

Table 2 σ_{pre}, σ_{post} and D values [see eqn. (6)] of the 1 at% La-doped $SrTiO_3$ samples implanted with $^{87}Sr^+$. σ_{pre} was obtained after the beam damage recovery anneal. t: annealing duration between the measurement of σ_{pre} and σ_{post}

	T/K	t/h	σ_{pre}/nm	σ_{post}/nm	D/m^2 s^{-1}
$SrTiO_3$(100)	1523	406	22.8	89.4	2.6E-21
$SrTiO_3$(100)	1573	196	34.0	135.8	1.2E-20
$SrTiO_3$(110)	1573	196	31.2	109.8	7.9E-21
$SrTiO_3$(111)	1623	176	23.1	170.0	2.2E-20
$SrTiO_3$(100)	1673	24	23.6	125.6	8.8E-20
$SrTiO_3$(110)	1673	24	27.2	110.3	6.6E-20
$SrTiO_3$(110)	1723	13.35	23.1	106.4	1.1E-19

^{88}Sr but at lower isotope fractions because of its lower natural abundance of 7.0%. At $t = 0$, the interface between the layer and the crystal is obviously not an ideal step profile. A broadening of the interface is observed, which was measured by differentiating the raw Sr isotope intensities over the depth and fitting a Gaussian function to the differentiated data. This is only an approximation, as the differentiated data shows a slight asymmetry which will be discussed later. The maximum of the Gauss distribution was taken to be the layer thickness, the full width at half maximum (FWHM) to be the interface broadening, respectively. The average layer thickness of all samples amounts to 43.6 ± 2.4 nm, the interface broadening to 13.3 ± 1.2 nm, showing that the reproducibility of the deposition method is very good.

To determine the origin of the observed deviation from the ideal step profile the instrumental effects during the SIMS measurement may be estimated. As was already shortly discussed in section 3.1, broadening of SIMS profiles is caused by surface roughness and waviness, atomic mixing due to ion bombardment and the information (emission) depth of the secondary ions.[36] The latter usually amounts to 0.3–0.4 nm and is therefore negligible in our case. The effect of surface roughness on a step profile can be described as an error function, the derivative of which is a Gaussian function with the measured roughness as the standard deviation parameter. The average surface roughness of all samples was measured *via* surface profiling during the crater depth measurements. It amounts to 3.2 ± 0.5 nm. The values at the crater bottom do not differ systematically from values measured at the surface, indicating that the surface is not significantly roughened by the sputtering process itself.

Atomic mixing, more precisely the recoil of target atoms or ions due to the ion bombardment during SIMS, depends on the primary ion energy, their incidence angle, their mass, and the

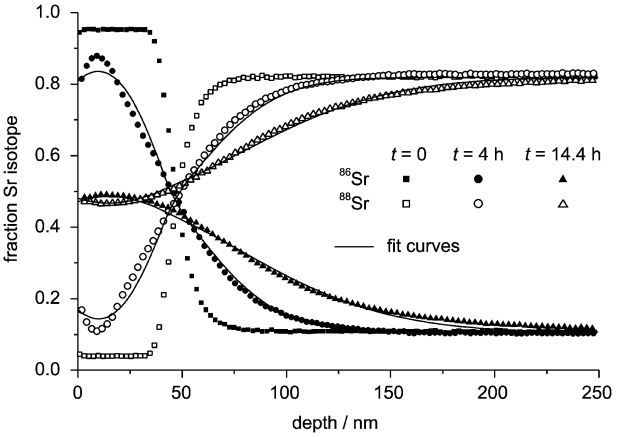

Fig. 3 ^{86}Sr and ^{88}Sr depth profiles recorded with SIMS on a 1 at% La-doped $SrTiO_3$(100) single crystal coated with a thin $^{86}SrTiO_3$ layer. t: annealing duration at $T = 1673$ K.

density and composition of the sample. Atomic mixing does not lead to a Gaussian but to an asymmetric redistribution with a steep leading and a slowly decreasing trailing edge which can be approximated by an exponential equation. The effect of atomic mixing was estimated using the MRI modelling software.[36] Starting from a step profile and using the measured roughness of 3.2 nm and an information depth of 0.4 nm, a fairly good agreement with the experimental data is obtained at a value of about 8.5 nm for the mixing zone width. This is a reasonable value, as SRIM calculations yield a depth value of 7.5 nm for the maximum of the Sr recoil distribution for the given SIMS analysis conditions using oxygen primary ions. It is therefore assumed that the interface broadening is solely caused by instrumental effects and that no tracer diffusion took place during the layer production. Comparable to the ion implanted samples, this instrumental broadening becomes less significant with increasing diffusion lengths.

After diffusion annealing, the expected exchange of Sr isotopes between layer and crystal is observed. In addition to the isotope exchange between layer and substrate, isotopic exchange of Sr also occurs at the layer surface (see Fig. 3). Two explanations are possible: Sr moves from and to the uncoated sample edge and backside (1) *via* fast surface diffusion and/or (2) by desorption/adsorption *via* the gas phase. As no significant difference could be detected in depth profiles recorded close to the edge or in the center of the samples, at least one of these processes seems to be fast enough to provide an excess of Sr at the surface, so that the incorporation of Sr into the lattice or the volume diffusion itself is the rate-limiting step. A verification using experimental data from the literature is difficult. Up to now, no Sr vapour pressure data is available for $SrTiO_3$ and only one study on surface diffusion on $SrTiO_3$ was published,[39] where the deepening of a grain boundary groove was measured by atomic force microscopy and therefore only the diffusivity of the slowest species, in the case of $SrTiO_3$ Ti, was determined. Also, the restructuring of the surface accompanied by a secondary phase growth (see section 1) leads to changes and local variations in the activities of Sr and Ti containing species at the surface making thermodynamical calculations based on vapour pressure data of SrO and TiO_2 highly speculative.

In Fig. 4, Sr isotope depth profiles of a 0.02 at% La-doped sample annealed at $T = 1773$ K are displayed. Depth profiles of undoped samples, which are not shown, look quite similar. In general, the Sr diffusivity is much lower in weakly or undoped $SrTiO_3$ than in strongly doped samples. In contrast to the strongly doped samples, no significant inward diffusion of Sr from the layer surface is observed. It seems therefore that the kinetics of the Sr surface transport or of the surface incorporation reaction depend even more on the dopant concentration than the Sr mobility in the crystal volume.

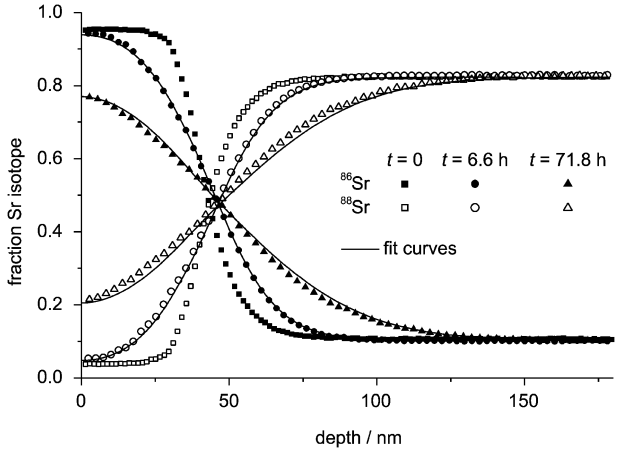

Fig. 4 ^{86}Sr and ^{88}Sr depth profiles recorded with SIMS on a 0.02 at% La-doped $SrTiO_3$(100) single crystal coated with a thin $^{86}SrTiO_3$ layer. *t*: annealing duration at $T = 1773$ K.

As the analytical solution of Fick's second law for a thick layer requires a step profile as the initial profile, the profiles were processed using an in-house software, which numerically solves Fick's second law for a measured initial profile and the respective annealing duration. Using a simplex algorithm, the two *D* values of the tracer layer and the bulk crystal, respectively, and the surface exchange coefficient are varied, until a best fit to the measured final profile is obtained. The layer–crystal interface was assumed as a boundary between the two different *D* values. As the experimental profiles are not discontinuous at the boundary and considering the interface broadening due to the SIMS analysis as discussed above, a boundary width of 13 nm was assumed. Within the boundary an exponential interpolation of the two *D* values was used. The ^{86}Sr and ^{88}Sr profiles were fitted simultaneously.

Figs. 3 and 4 show that the modelled and experimental curves agree well except for short annealing durations and strong La-doping. Here, a significant deviation from the modelled and experimental profiles is observed in the tracer layer. This is attributed to the fact that after deposition the tracer layer does not contain La and therefore possesses a low Sr vacancy concentration compared to the crystal volume (see eqn. (3)). The chemical diffusion of La into the layer at the beginning of the diffusion experiment is accompanied by a formation of Sr vacancies, leading to a Sr vacancy concentration gradient in the layer and a depth dependent Sr diffusivity. After prolonged annealing, the tracer layer possesses the same composition as the crystal substrate. Therefore, for short annealing and strong La-doping the diffusion model would have to be modified allowing for a depth dependent diffusivity in the layer. A complete diffusion model of the polycrystalline layer would also require the incorporation of grain boundary diffusion, which is virtually impossible to separate because of the low layer thickness. As these simplifications for the diffusion in the layer, however, do not affect the accuracy of the Sr volume diffusivities obtained for the single crystalline substrate, we will discuss only the latter.

To reach a sufficient diffusion length, at least two annealing steps had to be performed for most of the samples. The *D* values determined from the final measurements differ by ± 10 to 40% from the values obtained earlier for the respective samples. Therefore, no time or depth dependency of the Sr diffusivity is found. Because of the larger diffusion lengths the final values are considered to be the most accurate. These values are listed for all CSD coated samples in Table 3. They will be discussed together with the ion implantation results in the following section.

3.3. Diffusion coefficients

The Arrhenius diagram of all measured Sr volume diffusivities is displayed in Fig. 5. The results for the 1 at% La-doped samples show that, similar to the results for Ti and La,[28,29] no

Table 3 ^{86}Sr tracer diffusion: *D* values of the $SrTiO_3$ samples coated with the $^{86}SrTiO_3$ layer

	T/K	*t*/min	D/m^2 s^{-1}
Undoped	1573	31 260	9.4E-23
Undoped	1673	21 750	3.7E-22
Undoped	1773	4307	2.3E-21
0.02 at% La	1573	31 260	7.6E-23
0.02 at% La	1673	21 750	7.4E-22
0.02 at% La	1773	4307	2.6E-21
1 at% La	1573	1440	1.6E-20
1 at% La	1673	864	4.1E-20
1 at% La	1773	157	1.9E-19

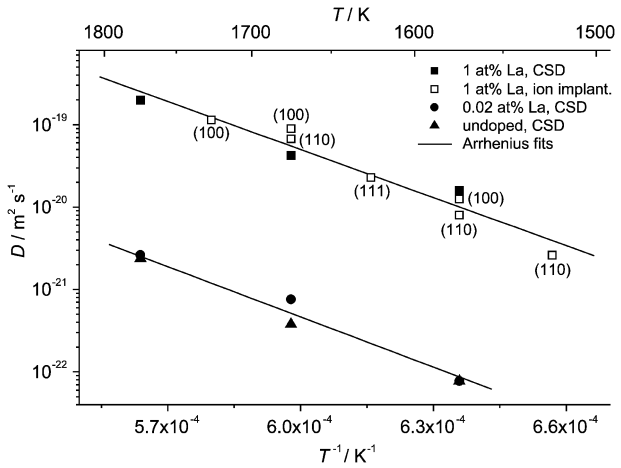

Fig. 5 Arrhenius diagram of the Sr volume diffusion coefficients listed in Tables 2 and 3. For the ion implanted samples the crystal orientations are given. All samples coated by CSD possess (100) orientation.

systematic dependence on the crystal orientation is observed. This is not surprising, considering the cubic crystal lattice of $SrTiO_3$. For 1 at% La-doped $SrTiO_3$, no significant difference between the diffusivities obtained with the two tracer deposition methods is found either. Hence, all values of both methods for 1 at% La-doped $SrTiO_3$ were used for an Arrhenius fit leading to the following pre-exponential factor and activation enthalpy:

$$D^{Sr}(1\ \text{at\% La}) = 10^{-7.6\pm1.0}\,\text{m}^2\,\text{s}^{-1}\exp\left(-\frac{(372\pm32)\text{kJ mol}^{-1}}{RT}\right)$$
$$\text{for } 1523\ \text{K} \le T \le 1773\ \text{K} \quad (8)$$

This corresponds to an activation enthalpy per atom of (3.9 ± 0.3) eV for 1 at% La-doped $SrTiO_3$.

The measured diffusivities for the weakly and undoped samples are considerably lower compared to the strongly doped samples. Within the experimental accuracy, the values determined for undoped and 0.02 at% La-doped $SrTiO_3$ by the CSD method appear to be similar. Using the D values from both dopant concentrations for an Arrhenius fit yields

$$D^{Sr}(\le 0.02\ \text{at\% La}) = 10^{-9.1\pm0.9}\,\text{m}^2\,\text{s}^{-1}\exp\left(-\frac{(389\pm30)\text{kJ mol}^{-1}}{RT}\right) \quad (9)$$
$$\text{for } 1573\ \text{K} \le T \le 1773\ \text{K},$$

corresponding to an activation enthalpy per atom of (4.0 ± 0.3) eV for ≤0.02 at% La-doped $SrTiO_3$. The activation enthalpy seems therefore to be dopant concentration independent.

This dependence of the volume diffusivity on the dopant concentration supports qualitatively the current defect chemical model for donor doped $SrTiO_3$ (see section 1) according to which under oxidizing conditions the donor, in this case La, is compensated by Sr vacancies [see eqn. (3)]. The correlation of Sr cation and Sr vacancy diffusion is given by:

$$D^{Sr} = \frac{[V''_{Sr}]}{[Sr^{\times}_{Sr}]}D^{V''_{Sr}}, \quad (10)$$

$[V''_{Sr}]/[Sr^{\times}_{Sr}]$ may be calculated for the 1 and 0.02 at% La-doped samples using eqn. (3). Assuming a constant $D^{V''_{Sr}}$ value, a ratio of D^{Sr} (1 at% La) ≈ $50D^{Sr}$ (0.02 at% La) is obtained. For the same ratio the experimental data yields values of about 100. Considering that an error of a factor of two is not uncommon in tracer diffusion experiments, this deviation is acceptable. Besides, because of the big difference in the Sr vacancy concentration the degree of interaction between the Sr vacancies may be significantly different, which was not taken into account for the above calculations.

In the case of the undoped samples, the Sr vacancy concentration has to be calculated in a different manner, as the undoped samples nominally do not contain La. By neglecting impurities, the Sr vacancy concentration is determined mainly by the partial Schottky equilibrium

$$Sr^{\times}_{Sr} + O^{\times}_{O} \Leftrightarrow V''_{Sr} + V^{\bullet\bullet}_{O} + SrO \quad (11)$$

with the Schottky constant

$$K_S(T) = [V''_{Sr}]\,[V^{\bullet\bullet}_{O}] = 3\times10^{42}\ \text{cm}^{-6}\exp(-2.5\ \text{eV}/k_BT) \quad (12)$$

The values for the preexponential factor and the activation enthalpy were taken from Helmbold[27] and Moos and Härdtl,[5] respectively. The Schottky constant depends slightly on the dopant concentration, which is included in an uncertainty of about one decade in the pre-exponential factor and of ±0.3 eV in the activation enthalpy.[5] The oxygen vacancy concentration can be calculated from the mass action law for eqn. (1), again using values of Moos and Härdtl:[5]

$$K_O(T) = [V^{\bullet\bullet}_{O}]n^2p(O_2)^{0.5} = 4.7\times10^{71}\ \text{cm}^{-9}\ \text{bar}^{0.5}\exp(-6.09\ \text{eV}/k_BT) \quad (13)$$

and $n = 2[V^{\bullet\bullet}_{O}]$ lead to

$$[V^{\bullet\bullet}_{O}] = \sqrt[3]{K_O/4p(O_2)^{0.5}}. \quad (14)$$

Inserting the obtained $[V^{\bullet\bullet}_{O}]$ values into eqn. (12) yields Sr vacancy concentrations between 1.5×10^{17} cm^{-3} at 1573 K and 2.2×10^{17} cm^{-3} at 1773 K. As these values are quite low, eqn. (10) gives ratios of D^{Sr} (1 at% La) ≈ 10^3 D^{Sr} (undoped) and D^{Sr} (0.02 at% La) ≈ $20D^{Sr}$ (undoped), which is much higher than experimentally observed but still within the error of the calculation, considering the error of one decade for K_S.

At very low dopant concentrations other defect equilibria than those regarded above may play a significant role for the creation of cation vacancies. The nominally undoped $SrTiO_3$ crystals contain a certain amount of impurities which is not exactly known. Impurity analyses of comparable commercial samples yield contents of $\le 3\times10^{16}$ cm^{-3} for Na, K, Si, and Fe and up to 7×10^{17} cm^{-3} for Al, Ca, and Ba. As elements acting as acceptors such as Fe and Al are generally more abundant than donor elements, the crystals are therefore probably slightly acceptor doped. However, this should cause a decrease rather than an increase in the Sr vacancy concentration. On the other hand, also other donor forming reactions are possible. For example, the formation of hydroxide ions on oxygen sites was observed in undoped and Fe-doped $SrTiO_3$ in hydrogen containing atmospheres:[40]

$$O^{\times}_{O} + 1/2\ H_{2(g)} \Leftrightarrow (OH)^{\bullet}_{O} + e' \quad (15)$$

However, as synthetic air was used in our experiments, the partial pressures of H_2 and H_2O in the atmosphere have both been low. For the undoped samples it is therefore not possible to calculate a reliable Sr vacancy concentration that could be used for an evaluation of the measured D^{Sr}. In the case of the 0.02 at% La-doped doped samples the difference between the dopant concentration (3.4×10^{18} cm^{-3}) and possible impurity concentrations is large enough so that impurities can be neglected.

An unexpected result is that for 0.02 at% La-doping, in contrast to the strongly doped samples, the D^{Sr} values measured with the CSD method are much higher than the maximum possible values obtained from the ion implantation method (see section 3.1). For example, the values determined for T = 1673 K amount to 5.2×10^{-22} m^2 s^{-1} for CSD and $\le 7.6\times10^{-23}$ m^2 s^{-1} for ion implantation, respectively. The reason for this substantial difference is not clear. We consider

the results from the CSD method to be more reliable, as in contrast to ion implantation the crystal lattice is not damaged by irradiation during tracer deposition. Furthermore, ion implantation introduces additional Sr into the lattice. At the given conditions, the Sr concentration is increased by more than 7 at% at the maximum of implantation. Following eqn. (3), the Sr vacancy concentrations amount to 2 and 0.04 at% for 1 and 0.02 at% La-doping, respectively, after equilibration under oxidizing conditions. Hence, in the case of strongly doped material at least a part of the excess Sr may be accommodated in Sr vacancies on recrystallisation of the radiation damage. As this is not possible for weakly doped material, a segregation and formation of secondary phases within the sample may occur, leading to the observed immobilization of the tracer.

Generally, the determined Sr diffusion coefficients are several orders of magnitude lower than the oxygen diffusion coefficients for the respective conditions.[27] Sr diffusion data for $SrTiO_3$ is very scarce in the literature. Up to now, only one Sr diffusion study was published, where ^{90}Sr radiotracer experiments were conducted at a $p(O_2)$ of 0.3–0.8 bar, using nominally undoped, slightly acceptor doped (100 ppm Al) $SrTiO_3$ single crystals.[25] Although, in principle, only at one temperature of 2148 K a D^{Sr} value of 2×10^{-18} m^2 s^{-1} was obtained, the authors argue that from Sr self-diffusion experiments for polycrystalline $SrTiO_3$ a lower limit for the activation enthalpy of 6.1 eV can be estimated, leading to a temperature dependency of D^{Sr} (undoped) $= 3.97 \times 10^{-4}$ m^2 s^{-1} $\exp(-6.1\ eV/k_BT)$.

Additionally, some data for the Sr vacancy diffusion coefficient was published. One experimental study deduced a value of $D^{V_{Sr}^g} = 5 \times 10^{-9}$ m^2 s^{-1} $\exp(-2.8\ eV/k_BT)$ from grain boundary capacitance measurements in 0.5 at% Nb-doped polycrystalline (Sr,Ca)TiO_3.[26] In another investigation, a value of $D^{V_{Sr}^g} = 10^{-7}$ m^2 s^{-1} $\exp(-3.5\ eV/k_BT)$ was obtained for a donor content of 0.2 at% comparing numerical data with experimental oxygen tracer diffusion profiles showing an irregular plateau shape.[17] The ambipolar diffusion of anion and cation defects allows in this case to monitor the evolution of the cation vacancy profile by anion tracer experiments. For dopant contents >0.2 at%, $D^{V_{Sr}^g}$ increases slightly.[17] Furthermore, computer simulation studies resulted in a value of 2.52 eV for the activation enthalpy of Sr vacancy diffusion.[12]

From these values for $D^{V_{Sr}^g}$, Sr diffusion coefficients were calculated using eqn. (10). All literature data are plotted together with the data of this work in the Arrhenius diagram in Fig. 6.

Because of the much higher activation energy of 6.1 eV, the D value of Rhodes and Kingery[25] increases more strongly with temperature, but the actual value at 1773 K is only *ca.* 1.2 times lower than our data for ≤ 0.02 at% La-doping, respectively. This difference is quite acceptable, considering that the values of Rhodes and Kingery were in fact deduced from experiments at a single temperature of 2148 K.

On the contrary, the values calculated from literature $D^{V_{Sr}^g}$ data are generally higher than our values. The best agreement is obtained with the data of Meyer *et al.*,[17] which deviate from our values by a factor of 2–3 at strong doping and 5–7 at weak doping. As these values were determined indirectly, this is a sufficient agreement, indicating that their method is helpful where direct cation diffusion measurements are not possible or very difficult. Another possible application would be to use their method prior to cation tracer diffusion experiments to estimate the required temperatures and annealing durations. A prerequisite is of course that the defect chemistry is known, that both cation and anion defects take part in the equilibration following a change in the atmosphere, and that the anion diffusivity is much higher compared to the cation diffusivity.

The values derived from Poignant and Abélard[26] exceed our data by a factor of 12 for strong doping and 1773 K to *ca.* 60 for weak doping and 1573 K. This might be related to the different chemical composition of their samples, containing a significant amount of Ca on the A site (with a Sr/Ca ratio of about 10) and minor quantities of Al and Si. Especially the high Ca content may be important, as pure $CaTiO_3$ possesses a different, orthorhombic distorted perovskite structure. Finally, because of their low activation enthalpy for Sr vacancy diffusion of 2.52 eV, the calculated values of Akhtar *et al.*[12] would lead to still higher D^{Sr} values, which are therefore not displayed in Fig. 6.

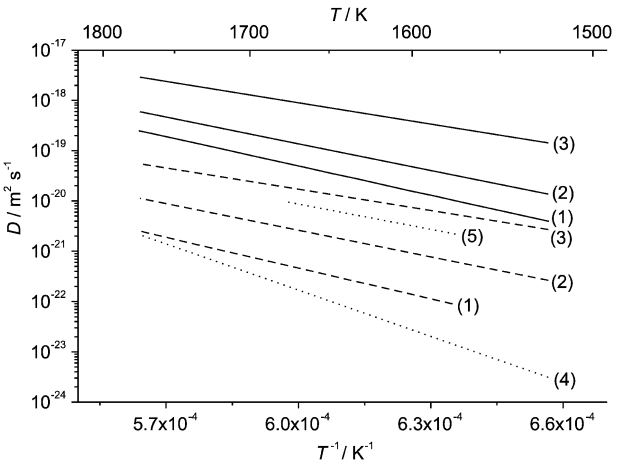

Fig. 6 Comparison of the D^{Sr} values determined in this work with literature data. Solid lines: 1 at% La-doping, dashed lines: 0.02 at% La-doping. For both dopant concentrations three data sets are displayed: (1) experimental data of this work, (2) D^{Sr} calculated from $D^{V_{Sr}^g}$ value of Poignant and Abélard,[26] (3) D^{Sr} calculated from $D^{V_{Sr}''}$ value of Meyer *et al.*[17] The dotted lines show additional data for comparison: (4) D^{Sr} values for undoped $SrTiO_3$ of Rhodes and Kingery,[25] (5) D^{Ti} for 1 at% La-doping.[29]

Fig. 6 also contains results for Ti tracer diffusion[29] obtained for 1 at% La-doped $SrTiO_3$ in the same manner as for the Sr ion implanted samples in this work. As with Sr, annealing of the weakly doped samples for several weeks did not lead to a measurable diffusion of the Ti tracer. A comparable dopant concentration dependency is observed, which is shifted to lower diffusivities by a factor of ≈ 5 compared to Sr. Because the low Ti vacancy concentrations (see section 1) and the high activation enthalpy of Ti vacancy diffusion of 11.6 eV,[12] Ti is also believed to move *via* Sr vacancies,[29] explaining the similar behaviour of Sr and Ti and the lower diffusivity of Ti compared to Sr.

Lastly, the determined Sr diffusion coefficients are about a decade lower than La diffusion coefficients for the same material at 1 at% La-doping and 1573 K.[28] Hence, the La diffusion coefficient is comparable to the Sr vacancy diffusion coefficient which is supported by the relation $D^{La} \approx 0.5\ D^{V_{Sr}^g}$ following from the combination of eqn. (3) and (10). Again, the La diffusivity increases with the doping concentration indicating a similar, strontium vacancy mediated transport mechanism.

Acknowledgements

We are grateful to M. Frerichs for the XPS measurements, F. Jomard for performing some of the SIMS analyses and to the Deutsche Forschungsgemeinschaft (DFG) for financial support.

References

1 Y.-M. Chiang, D. P. Birnie III and W. D. Kingery, *Physical Ceramics. Principles for Ceramic Science and Engineering*, Wiley, New York, 1997, pp. 225–233.

2 R. A. De Souza, J. Fleig, R. Merkle and J. Maier, *Z. Metallkd.*, 2003, **94**, 218.
3 K. Szot, W. Speier, U. Breuer, R. Meyer, J. Szade and R. Waser, *Surf. Sci.*, 2000, **460**, 112.
4 A. Gunhold, K. Gömann, L. Beuermann, V. Kempter, G. Borchardt and W. Maus-Friedrichs, *Surf. Sci.*, 2004, **566–568**, 105.
5 R. Moos and K. H. Härdtl, *J. Am. Ceram. Soc.*, 1997, **80**, 2549.
6 F. A. Kröger and H. J. Vink, *Solid State Phys.*, 1956, **3**, 307.
7 U. Balachandran and N. G. Eror, *J. Mat. Sci.*, 1982, **17**, 2133.
8 U. Balachandran and N. G. Eror, *J. Electrochem. Soc.*, 1982, **129**, 1021.
9 W. Menesklou, *Kompensationsmechanismen der Überschußladung in lanthandotiertem Barium- und Strontiumtitanat*, Fortschritt-Berichte, VDI, VDI Verlag, Düsseldorf, Germany, 1997, vol. 5, 481.
10 T. Y. Tien and F. A. Hummel, *Trans. Br. Ceram. Soc.*, 1967, **66**, 233.
11 R. Moos, T. Bischoff, W. Menesklou and K. H. Härdtl, *J. Mat. Sci.*, 1997, **32**, 4247.
12 M. J. Akhtar, Z.-U.-N. Akhtar, R. A. Jackson and C. R. A. Catlow, *J. Am. Ceram. Soc.*, 1995, **78**, 421.
13 K. Wright and G. D. Price, *J. Geophys. Res.*, 1993, **98**, 22245.
14 S. N. Ruddlesden and P. Popper, *Acta Crystallogr.*, 1958, **11**, 54.
15 W. Menesklou, H.-J. Schreiner, K. H. Härdtl and E. Ivers-Tiffée, *Sensors Actuatuators B*, 1999, **59**, 184.
16 M. A. McCoy, R. W. Grimes and W. E. Lee, *Philos. Mag. A*, 1997, **75**, 833.
17 R. Meyer, R. Waser, J. Helmbold and G. Borchardt, *Phys. Rev. Lett.*, 2003, **90**, 105901.
18 R. Meyer, R. Waser, J. Helmbold and G. Borchardt, *J. Electroceram.*, 2002, **9**, 101.
19 Han Wei, W. Maus-Friedrichs, G. Lilienkamp, V. Kempter, J. Helmbold, K. Gömann and G. Borchardt, *J. Electroceram.*, 2002, **8**, 221.
20 A. Gunhold, K. Gömann, L. Beuermann, M. Frerichs, G. Borchardt, V. Kempter and W. Maus-Friedrichs, *Surf. Sci.*, 2002, **507–510**, 447.
21 R. Meyer, K. Szot and R. Waser, *Ferroelectrics*, 1999, **224**, 751.
22 K. Szot and W. Speier, *Phys. Rev. B*, 1999, **60**, 5909.
23 A. Gunhold, L. Beuermann, M. Frerichs, V. Kempter, K. Gömann, G. Borchardt and W. Maus-Friedrichs, *Surf. Sci.*, 2003, **523**, 80.
24 A. Gunhold, K. Gömann, L. Beuermann, G. Borchardt, V. Kempter and W. Maus-Friedrichs, *Anal. Bioanal. Chem.*, 2003, **375**, 924.
25 W. H. Rhodes and W. D. Kingery, *J.Am. Ceram. Soc.*, 1966, **49**, 521.
26 F. Poignant and P. Abélard, *Key Eng. Mater.*, 1997, **132–136**, 1337.
27 J. Helmbold, Einfluss der Dotierungskonzentration auf den Sauerstofftransport in donatordotiertem $SrTiO_3$, PhD Thesis, Technische Universität Clausthal, Germany, 2001.
28 K. Gömann, G. Borchardt, A. Gunhold, W. Maus-Friedrichs, B. Lesage, O. Kaïtasov and H. Baumann, *Mat. Res. Soc. Proc.*, 2003, **756**, EE3.1.1.
29 K. Gömann, G. Borchardt, A. Gunhold, W. Maus-Friedrichs and H. Baumann, *Phys. Chem. Chem. Phys.*, 2004, **6**, 3639.
30 S. M. M. Ramos, B. Canut, P. Moretti, P. Thevenard and D. Poker, *Thin Solid Films*, 1995, **259**, 113.
31 F. Wang, M. Badaye, Y. Yoshida and T. Morishita, *Nucl. Instrum. Methods Phys. Res., Sect. B*, 1996, **118**, 547.
32 U. Hasenkox, S. Hoffmann and R. Waser, *J. Sol-Gel Sci. Technol.*, 1998, **12**, 67.
33 S. Hoffmann and R. Waser, *J. Eur. Ceram. Soc.*, 1999, **19**, 1339–1343.
34 H. Ryssel and I. Ruge, *Ion Implantation*, Wiley, Chichester, 1986, p. 14.
35 http://www.srim.org, see also: J. F. Ziegler, H. Biersack and U. Littmark, *The Stopping and Range of Ions in Solids*, Pergamon, Oxford, 1985, pp. 202–262.
36 S. Hofmann, *Rep. Prog. Phys.*, 1998, **61**, 827–888.
37 P. Fielitz, G. Borchardt, M. Schmücker and H. Schneider, *Phys. Chem. Chem. Phys.*, 2003, **5**, 2279.
38 H. Kaiser and H. Specker, *Z. Anal. Chem.*, 1956, **149**, 46.
39 M. Jin, E. Shimada and Y. Ikuma, *J. Mat. Res.*, 1999, **14**, 2548–2553.
40 R. Waser, *Z. Naturforsch., A*, 1987, **42**, 1357.

